Quantitative Measurement with Scanning Thermal Microscope by Preventing the Distortion Due to the Heat Transfer through the Air

Kyeongtae Kim,[†] Jaehun Chung,[†] Gwangseok Hwang,[†] Ohmyoung Kwon,[†,*] and Joon Sik Lee[‡]

[†]Department of Mechanical Engineering, Korea University, 1 Anam-dong-5-ga Sungbuk-gu, Seoul 136-701, Korea, and [‡]School of Mechanical & Aerospace Engineering, Seoul National University, 599 Gwanak-ro, Gwanak-gu, Seoul 155-744, Korea

ABSTRACT

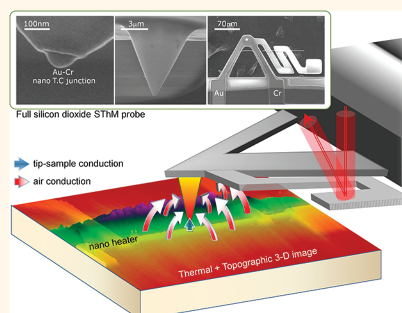

Because of its high spatial resolution, scanning thermal microscopy (SThM) has been developed quite actively and applied in such diverse areas as microelectronics, optoelectronics, polymers, and carbon nanotubes for more than a decade since the 1990s. However, despite its long history and diverse areas of application, surprisingly, no quantitative profiling method has been established yet. This is mostly due to the nonlocal nature of measurement by conventional SThM: the signal measured by SThM is induced not only from the local heat flux through the tip−sample thermal contact but also (and mostly) from the heat flux through the air gap between the sample and the SThM probe. In this study, a rigorous but simple and practical theory for quantitative SThM for local measurement is established and verified experimentally using high-performance SThM probes. The development of quantitative SThM will make possible new breakthroughs in diverse fields of nanothermal science and engineering.

KEYWORDS: scanning thermal microscopy · thermocouple probe · quantitative profiling · temperature · thermal conductivity

The scanning thermal microscope (SThM) is a type of scanning probe microscope (SPM) that maps out the temperature and/or the thermal property by scanning a sharp SThM probe with a temperature sensor at the tip.[1,2] Because of its high spatial resolution, SThM has been developed quite actively and applied in such diverse areas as microelectronics,[3−6] optoelectronics,[7−9] polymers,[10−12] and carbon nanotubes[13,14] for more than a decade since the 1990s. However, despite its long history and diverse areas of application, surprisingly, no quantitative profiling method has been established yet. This is mostly due to the nonlocal nature of measurement by conventional SThM: the signal measured by SThM is induced not only from the local heat flux through the tip−sample thermal contact but also (and mostly) from the heat flux through the air gap between the sample and the SThM probe.[15]

Surprisingly, it took a lot of time and effort to understand and ascertain the nonlocal nature of measurement by SThM. For example, Luo *et al.* presumed that the heat flux through the air gap between the SThM probe and the sample is negligible and that heat flows from the sample to the SThM probe only through the tip−sample thermal contact.[16] According to this presumption, the actual temperature of the sample, T_s, is proportional to the temperature measured by the SThM probe in the contact mode, T_c; that is

$$T_s(x) = (1+\phi)T_c(x) \quad (1)$$

where ϕ is the ratio of the thermal resistance of the tip−sample contact to that of the cantilever, and x is the location of the tip−sample contact on the sample.

Later, however, some experimental results from the same research group unexpectedly negated the validity of eq 1. For example, even if the temperature of the sample was the same, the temperature rise measured by SThM, depending on the size of the sample, varied by more than 10 times. Furthermore, the temperature profile around an electrically heated metal line measured by SThM could not be fitted to that obtained

* Address correspondence to omkwon@korea.ac.kr.

Received for review July 14, 2011 and accepted October 15, 2011.

Published online October 15, 2011
10.1021/nn2026325

© 2011 American Chemical Society

from modeling, by just shifting or stretching.[15] This means that the measured temperature profile was distorted due to the nonlocal nature of the measurement.

For quantitative thermal conductivity profiling, however, the nonlocal nature of the measurement by SThM does not seem to have been fully ascertained. For example, Ruiz *et al.* argued that the local thermal conductivity can be measured quantitatively from Q_s, which is the heat going into the sample from the electrically heated SThM probe and that Q_s can be obtained by

$$Q_s = Q_{total} - Q_{air} \quad (2)$$

where Q_{total} is the total heat dissipated into the probe when the tip is placed in contact with the sample, and Q_{air} is the heat dissipated into the probe when the tip is in the air.[17]

The argument by Ruiz *et al.* would be correct if the Q_s obtained in the above manner were the heat going into the sample through the tip–sample thermal contact. However, since Q_{air} increases rapidly as the probe approaches the sample, the Q_s obtained in the above manner is much larger than the heat going into the sample through the tip–sample thermal contact. In order to obtain Q_s which is the heat going into the sample through the tip–sample thermal contact, Q_{air} should be measured not when the tip is in the air but just before the tip makes contact with the sample surface.

Although a linear relationship between Q_s obtained in the above manner and the thermal conductivity has been presented for a number of materials as evidence of quantitative measurement, this observation, unfortunately, was made only on apparently homogeneous samples. If the possible distortion of the thermal conductivity profile due to the nonlocal nature of measurement had been considered, profiling of a sample with a known thermal conductivity distribution—and not point measurement on homogeneous samples—should have been presented as evidence of quantitative local measurement.

To recapitulate, for quantitative local measurement, one should completely remove the influence of the heat flux through the air gap, which prevents local measurement, and relate the local temperature or thermal conductivity to the thermal signal due to only the heat flux through the tip–sample thermal contact, which is local. This is regardless of whether one uses the SThM probe in a passive mode (as a thermometer) to measure the local temperature or in an active mode (as a heater and thermometer) to measure the local thermal conductivity. Furthermore, as evidence of quantitative measurement, due to the possible distortion of the measured profile, instead of measurement at certain points, profiling of the sample with a known temperature or thermal conductivity distribution should be presented.

In this study, we focus only on the quantitative measurement of the temperature (specifically, the steady temperature distribution) either in active or in passive mode. However, in order to avoid any confusion, we need to explain the quantitative measurement of the amplitude and the phase lag distributions of the steady periodic temperature field (which is, confusingly, sometimes referred to as the temperature measurement).

While the quantitative measurement of the steady temperature distribution has not previously been reported, as noted above, Kwon *et al.* developed the scanning thermal wave microscopy (STWM), a technique that can map out the amplitude and phase lag distribution of the steady periodic temperature field quantitatively with an SThM probe.[18] They demonstrated that if the heating frequency of the steady periodic temperature field is sufficiently high (>1.6 kHz), then the amplitude and phase lag distribution of the steady periodic temperature field can be mapped out quantitatively. They explained that this is due to the fact that the influence of the thermal wave transferred through the air gap and the cantilever of the SThM probe becomes negligible compared to that of the thermal wave transferred to the sensor directly through the tip–sample thermal contact because the penetration depth of the thermal wave decreases with increasing heating frequency.

Recently, Grosse *et al.* reported the measurement of "the temperature distribution" with a spatial resolution of ~10 nm by scanning Joule expansion microscopy (SJEM), a technique originally developed by Majumdar *et al.*[19,20] However, it should be noted that it was not exactly the steady temperature distribution that they measured, but the amplitude distribution of the steady periodic temperature field with a heating frequency of 65 kHz. Although SJEM can measure only the amplitude distribution of the steady periodic temperature field of very high heating frequency (>10 kHz), requiring very elaborate calibration and fitting procedures and seeming to have relatively large noise (~250 mK), which can deteriorate its spatial resolution, SJEM has the advantage that it does not require a specialized probe such as the one used in this study.

Sadat *et al.* also reported that they were able to measure the temperature distribution with a spatial resolution of ~100 nm if the sample surface is coated with a ~30 nm thin gold film.[21] However, it should again be pointed out that it was not the steady temperature distribution that is measured here, but rather the amplitude distribution of the steady periodic temperature field with a heating frequency of 70 Hz. In principle, it might be possible to apply this technique to the measurement of the steady temperature distribution. However, in their report, only the measurement of the amplitude distribution of the steady periodic temperature field was discussed. Although

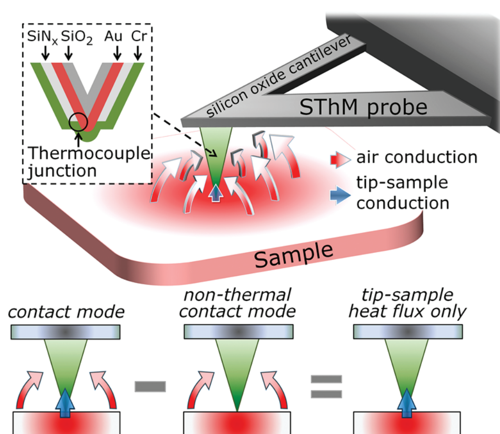

Figure 1. Principle of quantitative thermal profiling. The SThM probe with a nanothermocouple junction integrated at the end of the tip as shown in the inset is mounted on an AFM and scans on the same line in both the contact mode and the nonthermal contact mode. Then, the difference between the signals obtained in the two modes is due only to the heat flux through the tip−sample thermal contact.

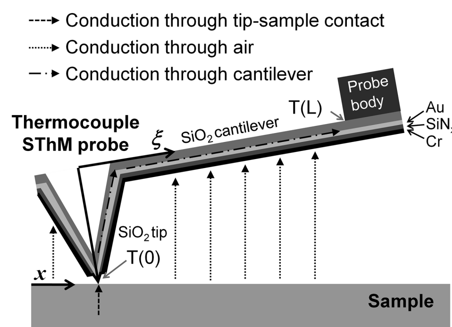

Figure 2. Schematic diagram of the SThM probe in contact with the sample and various heat transfer paths around the probe to the thermocouple junction at the end of the tip; ξ represents a position in the probe and is set to zero at the end of the tip, while x means the position at which the tip−sample contact is made.

the amplitude distribution of the steady periodic temperature field can be disturbed by the gold coating, this technique has a similar advantage to SJEM in that it does not require a specialized probe such as the one used in this study.

Since it has already been demonstrated that the amplitude and phase lag distribution of the steady periodic temperature field (which is, confusingly, sometimes referred to as the temperature) can be mapped out quantitatively by using the SThM probe without the distortion due to the heat transfer through the air gap,[18] in this study, we focus on the quantitative measurement of the steady temperature and the thermal conductivity distribution.

THEORY

For quantitative profiling, we suggest a method that is graphically explained in Figure 1. First, while a SThM probe scans in the contact mode, T_c is obtained from the temperature sensor integrated at the tip of the probe. Obviously, T_c is due to both the heat flux through the tip−sample thermal contact, Q_{ts}, and the heat flux through the air gap, Q_{air}. Second, while the SThM probe scans in the nonthermal contact mode, which is an imaginary scanning mode in which Q_{ts} is zero and Q_{air} is the same as that in the contact mode, T_{nc} is obtained from the temperature sensor. Then, the difference between T_{nc} and T_c is due only to Q_{ts}. Hence, one can predict that the difference is proportional to Q_{ts}

$$Q_{ts} = C(T_{nc}(x) - T_c(x)) \tag{3}$$

where C is a proportionality constant whose dimension is [W/K], and x is the location of the tip−sample contact.

However, one might think that physical intuition is insufficient to guarantee the validity of eq 3 because both T_{nc} and T_c can be affected by not only Q_{ts} but also several other factors, including heat conduction in the tip and the cantilever of the probe, heat convection through the air gap, heat convection to other surroundings, and heat generation in the probe. Hence, by analyzing the governing equations and the boundary conditions for the temperature distributions in the probe during the contact mode scan and the nonthermal contact mode scan, we prove eq 3 rigorously as follows. The following derivation is an expanded version of our previous derivation[22] so that it can include the influence of both heat generation in the probe and heat flux to the surroundings except the sample. The generalization of this theory allows its expansion to quantitative thermal conductivity measurements.

The structure of the thermocouple SThM probe and the coordinates for theoretical analysis are depicted in Figure 2. The governing equation for the temperature distribution during the contact mode scan is

$$\frac{d}{d\xi}\left[\sum A_i(\xi)k_i\frac{dT_c(\xi)}{d\xi}\right] - p(\xi)h_{eff}(\xi)[T_c(\xi) - T_s(\xi)] - p_\infty(\xi)h_\infty(\xi)[T_c(\xi) - T_\infty(\xi)] + g(\xi) = 0 \tag{4}$$

where ξ represents a position in the probe, T_c is the local temperature in the probe during the contact mode, A_i is the cross section of the ith composing layer, k_i is the thermal conductivity of the material composing the ith layer, p is the perimeter of the probe related to the surface that exchanges heat flux with the sample, h_{eff} is the effective heat transfer coefficient between the probe and the sample, T_s is the local temperature of the sample, p_∞ is the perimeter of the probe related to the surface that exchanges heat flux with the surroundings except the sample, h_∞ is the effective heat transfer coefficient between the probe and the surroundings except the sample, and g is the heat generation per unit length of the probe.

The boundary condition for eq 4 is

$$\sum A_i(0)k_i\frac{dT_c(0)}{d\xi} = Q_{ts} = G_{ts}(T_c(0) - T_s(0)),\ T_c(L) = T_b \quad (5)$$

where G_{ts} is the tip−sample thermal conductance, and the local temperature in the probe at $\xi = L$ at which the cantilever is connected to the probe body is assumed to be equal to the temperature of the probe body, T_b.

The governing equation for the temperature distribution during the nonthermal contact mode scan is

$$\frac{d}{d\xi}\left[\sum A_i(\xi)k_i\frac{dT_{nc}(\xi)}{d\xi}\right] - p(\xi)h_{eff}(\xi)[T_{nc}(\xi) - T_s(\xi)] - p_\infty(\xi)h_\infty(\xi)[T_{nc}(\xi) - T_\infty(\xi)] + g(\xi) = 0 \quad (6)$$

where T_{nc} is the local temperature in the probe during the nonthermal contact mode.

The boundary condition for eq 6 is

$$\sum A_i(0)k_i\frac{dT_{nc}(0)}{d\xi} = 0,\ T_{nc}(L) = T_b \quad (7)$$

Now, by subtracting eq 6 from eq 4, following the measurement principle, one can obtain

$$\frac{d}{d\xi}\left[\sum A_i(\xi)k_i\frac{dT_j(\xi)}{d\xi}\right] - [p(\xi)h_{eff}(\xi) + p_\infty(\xi)h_\infty(\xi)]T_j(\xi) = 0 \quad (8)$$

where T_j is $T_c - T_{nc}$, which is the temperature jump due to Q_{ts}.

In a similar manner, by subtracting eq 7 from eq 5, one can obtain the boundary condition for eq 8 as

$$\sum A_ik_i\frac{dT_j(0)}{d\xi} = Q_{ts} = G_{ts}(T_c(0) - T_s(0)),\ T_j(L) = 0 \quad (9)$$

The significance about eq 8 and its boundary condition eq 9 is that, unlike eqs 4 and 6, they are homogeneous. Therefore, the solution $T_j(\xi)$ is linearly proportional to Q_{ts} in the entire domain. This linear relationship also holds at the end of the tip ($\xi = 0$). Hence, one can obtain

$$Q_{ts} = C(0)(T_c(0) - T_{nc}(0)) \quad (10)$$

where $C(0)$ is a proportionality constant whose dimension is [W/K].

Equation 10 holds regardless of the location of the tip−sample contact; during the derivation leading to eq 10, we did not make any assumption about the position of the tip−sample contact on the sample, and the temperature measured by a SThM probe is practically the temperature at the end of the tip ($\xi = 0$) since the thermocouple junction is located very close to the end of the tip. Therefore, when it is obvious that one considers only the temperature measured by SThM, without confusion, one can rewrite eq 10 as eq 3.

Now, we need to relate Q_{ts} to T_s. Obviously, during the contact mode, Q_{ts} is proportional to the difference between T_c and T_s

$$Q_{ts} = G_{ts}(T_c(x) - T_s(x)) \quad (11)$$

where G_{ts} is the tip−sample thermal conductance.

Then, the combination of eqs 3 and 11 yields

$$T_s(x) = T_c(x) + \varphi(T_c(x) - T_{nc}(x)) \quad (12)$$

where φ is a dimensionless constant defined as C/G_{ts}. Equation 12 indicates that, in order to obtain the real T_s, both T_c and T_{nc} should be measured. A caveat in using eq 12 to determine the quantitative temperature distribution is that one should operate the probe in the passive mode since T_s can be disturbed by Q_{ts} in the active mode.

For quantitative conductivity profiling, we expand this theory further. In general, the following relations hold for Q_{ts}, the spreading thermal resistance R_{th}, and the local thermal conductivity k:

$$Q_{ts} = \frac{1}{R_{th}}(T_s - T_\infty),\ R_{th} = \frac{1}{4ak} \quad (13)$$

where T_∞ is the temperature of the surroundings and a is the radius of the tip−sample thermal contact.[23]

Then, the combination of eqs 3, 12, and 13 yields

$$\frac{1}{k} = \frac{4a}{C}\left[\frac{T_c - T_\infty}{T_{nc} - T_c} - \frac{C}{G_{ts}}\right] \quad (14)$$

which indicates that, in order to obtain the thermal conductivity distribution, both T_c and T_{nc} should be measured.

RESULTS AND DISCUSSION

The experimental setup for quantitative temperature profiling is depicted in Figure 3a, and the scanning electron micrographs of the SThM probe are in Figure 3b. The theory developed in this study reveals that, for local measurement, a highly sensitive SThM probe that can respond to Q_{ts}, which is extremely small, is required. In order to maximize the sensitivity of the probe, the tip and the cantilever of the probe are made of silicon dioxide, whose thermal conductivity is very low (~1.2 W/m·K), and the tip is increased to 12 μm to minimize the influence of the heat flux through the air gap (see the Supporting Information).

To determine φ in eq 12, as shown in Figure 3c, the temperature of the tip is monitored, while the tip of the probe approaches a gold line heater, whose temperature is measured from its temperature coefficient of resistance (TCR). Until the tip touches the heater, the temperature of the tip rises continuously due to the increasing heat transfer through the air. When the tip touches the sample, the temperature of the tip jumps from T_{nc} to T_c due to Q_{ts}. The temperature jumps are measured at several different temperatures of the sample, and the results are summarized in Figure 3d. The φ for this particular probe is 10.9 K/K.

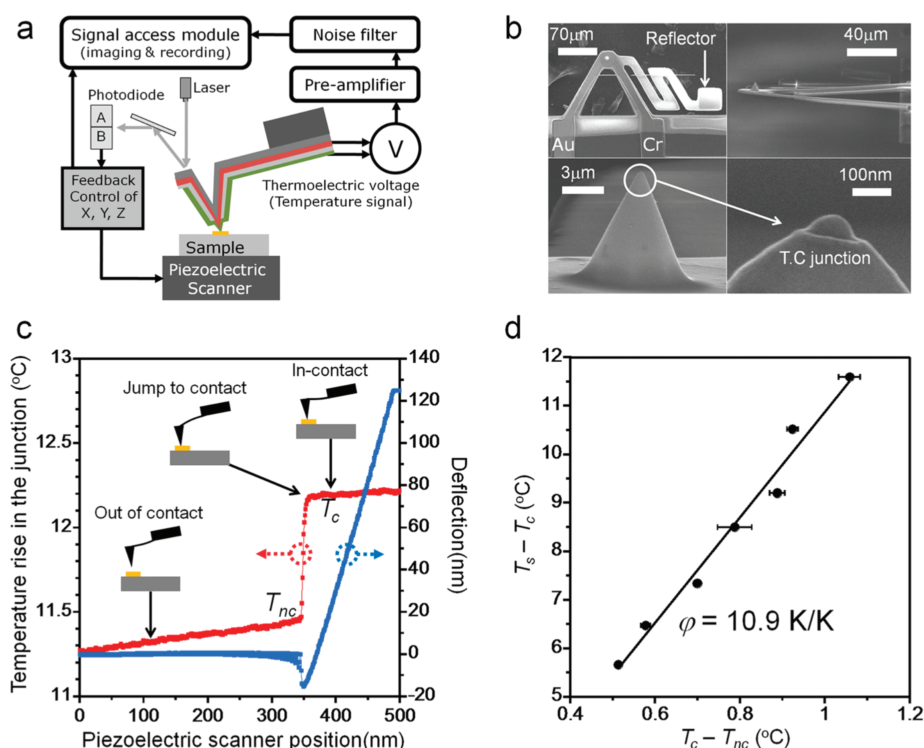

Figure 3. Experimental setup and its calibration for quantitative temperature profiling. (a) Experimental setup. (b) Scanning electron micrographs of the thermocouple probe. The diameter of the thermocouple junction is about 200 nm, and the radius of the tip is about 100 nm. (c) As the tip approaches the sample, the temperature of the tip rises gradually due to the heat transfer through the air. When the tip makes contact with the sample, the temperature of the tip jumps from T_{nc} to T_c due to the heat flux through the tip−sample contact. (d) Temperature jumps measured at several different temperatures of the sample. The slope of the graph, which is φ, is 10.9 K/K for this particular probe. The error bars are calculated from the standard deviation in the temperature measured by the thermocouple SThM probe.

Although T_{nc} at a certain point on the sample can be obtained from the experiment above, for the effective use of eq 12, however, continuous profiling of T_{nc} is necessary. Previously,[22] instead of T_{nc}, we used the temperature measured while the tip scanned at a certain height above the sample. The temperature measured in that manner involved considerable error due to the incomplete removal of the heat transfer through the air.

In order to eliminate this error, in this study, we obtain two temperature profiles by scanning the probe along the same scan line at two different heights above the sample surface using the topography data obtained in contact mode; then, at each position of the sample, by linearly extrapolating the two temperature values at two different heights with respect to the height, we obtain T_{nc}, which corresponds to the temperature measured at the height of zero without Q_{ts}. Since the temperature of the tip varies quite linearly with the height near the sample surface, as one can see from Figure 3c, T_{nc} obtained in this manner seems quite accurate.

For a demonstration of quantitative temperature profiling, we need a heater whose temperature can be controlled and monitored accurately, and we should make this heater as small as possible. The smallest we have made is a 300 nm wide gold line patterned in a four-probe configuration, whose temperature can be monitored through its TCR. The topography of the heater and the scan line across it are shown in Figure 4a.

The measured T_c and T_{nc} and the T_s derived from them through eq 12 are shown in Figure 4b. For comparison, we obtain the temperature profile around the heater through finite element modeling from the power dissipated in the heater; we then shift the profile until the temperature of the heater itself matches with the temperature measured by the TCR of the heater line, T_{TCR}. While T_{nc} increases gradually around the heater, T_c fluctuates sharply in an N-shape at the edge of the heater. This abrupt change of T_c is due to the change in G_{ts} caused by the rapid change in the tip−sample contact area at the edge of the heater, as illustrated in the bottom of Figure 4a. Although both the absolute value and the profile of T_c are quite different from the results of modeling, the T_s that is derived using eq 12 accords very well with the results of modeling, except for the abrupt N-curve at the edge.

Now that the effectiveness of eq 12 is demonstrated, we move on to quantitative thermal conductivity profiling. Traditionally, the thermocouple probe has been used mostly for temperature measurement and thermoresistive probes mostly for thermal property measurement. While the thermocouple probe has

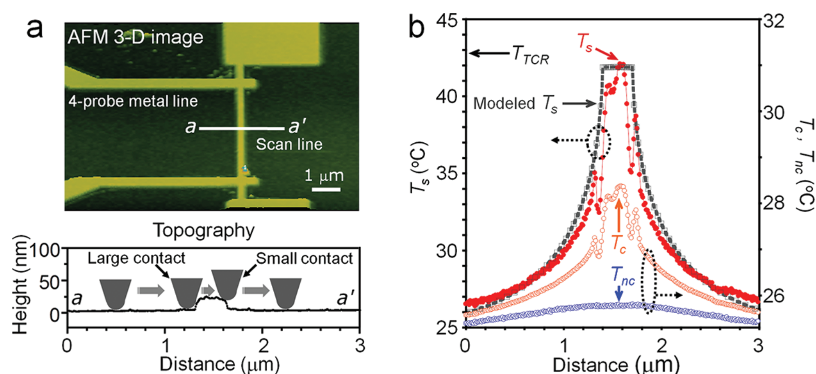

Figure 4. Demonstration of quantitative temperature profiling. (a) AFM image of a 300 nm wide and 25 nm thick gold line patterned in a four-probe configuration (top). The tip−sample thermal contact area abruptly changes near the edge of the heater (bottom). (b) Comparison of the measured T_c and T_{nc}, the T_s derived from them through eq 5, and the T_s modeled from the power dissipated in the heater and shifted until the temperature of the heater itself becomes the same as T_{TCR}.

been recognized as a passive thermometer, only the thermoresistive probe has been considered an active sensor that can generate heat and measure the temperature simultaneously.[2]

However, for local measurement, the thermocouple probe has advantages over the thermoresistive probe in terms of both spatial resolution and sensitivity. First, if the sensing resistor of the thermoresistive probe, which detects the local temperature from its resistance change, is shortened to enhance the spatial resolution, the sensitivity of the sensor deteriorates since the signal from the sensing resistor decreases due to the reduced resistance of the sensing resistor. On the other hand, even if the size of the sensing thermocouple is reduced to enhance the spatial resolution, the signal from the sensor does not decrease because the thermocouple is a point sensor in principle.

Second, to improve the sensitivity of a thermometer, the sensing part should be thermally insulated as much as possible. However, the thermoresistive probe requires a much thicker electrical lead than the sensing resistor since the electrical resistance of the lead should be much smaller than that of the sensing resistor. The thick electrical lead prevents proper thermal insulation of the sensing resistor and lowers its sensitivity. On the other hand, the thermocouple probe does not require a thick electrical lead; through appropriate thermal design, the sensing thermocouple can be properly insulated.

Since the thermocouple probe, compared with the thermoresistive probe, is more advantageous in terms of improving both the sensitivity and the spatial resolution through the thermal isolation and the size reduction of the sensing part, we use the thermocouple probe in the active mode for thermal conductivity profiling.

The active-mode operation of the thermocouple probe can be achieved in either an ac or dc manner. Previously, Rho *et al.* developed the active-mode operation in an ac manner, viz., "the 2ω method", in which the thermocouple junction of the probe is heated by an ac current of angular frequency ω through the Joule effect and the amplitude of periodic temperature oscillation is monitored by measuring the thermoelectric voltage at the frequency of 2ω that is induced by the periodically oscillating temperature at the junction.[24,25] Though it demonstrated improved sensitivity and spatial resolution, the 2ω method remains a qualitative measurement technique.

In this study, we use the active-mode operation in a dc manner, in which the thermocouple junction of the probe is heated by an ac current of high frequency through the Joule effect and the temperature of the junction is monitored by measuring the dc thermoelectric voltage from the junction. If the frequency of the ac current is high enough (>100 kHz) with respect to the thermal time constant of the thermocouple junction (>1 ms), the periodic component of the temperature variation of the junction becomes almost negligible. Even though the driving current is ac, the thermoelectric voltage generated from the junction is dc; hence, the temperature of the junction can be monitored without the interference of the driving ac bias.

The experimental setup for the active-mode operation of the thermocouple SThM probe is depicted in Figure 5. The experimental setup consists of a function generator, a preamplifier, a notch-filter, a signal access module (SAM), a Wheatstone bridge circuit, a SThM probe, and a scanning probe microscope (SPM).

Though very small, an unwanted dc drift voltage often accompanies the ac driving bias. By using a Wheatstone bridge circuit, we completely remove the influence of the unwanted dc drift voltage, which interferes with the measurement of the dc thermoelectric voltage generated from the thermocouple junction. One can check whether the unwanted dc drift voltage is completely removed by swapping the thermocouple leads connected to the Wheatstone bridge. If the absolute value of the thermoelectric voltage remains the same, it means that the dc drift voltage has been completely removed. The relationship

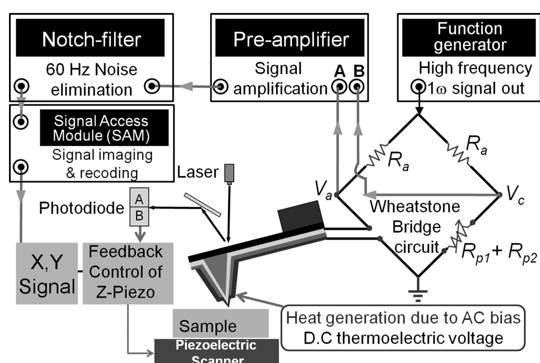

Figure 5. Schematic diagram of the experimental setup for the active-mode operation of the thermocouple SThM probe. The signal from the bridge circuit is amplified by the preamplifier. A noise filter is used to maximize the signal-to-noise ratio by reducing the 60 Hz harmonic noise. The filtered signal is fed into the signal access module (SAM) and becomes simultaneously available with the topography signal of the atomic force microscope (AFM). A dc power supply is used to heat the sample.

between the thermoelectric voltage generated from the thermocouple junction and the voltage extracted from the bridge circuit can be obtained through simple node-voltage analysis as

$$V_{TE} = \frac{(V_a - V_c)(R_a + R_{p1} + R_{p2})}{R_a} \quad (15)$$

Then, the signal is amplified, filtered, and fed into the SAM and becomes simultaneously available with the topography signal of the AFM.

The heating of the thermocouple junction of the SThM probe is not exactly point-heating because the junction of the probe is heated by the Joule effect. However, the current density increases approaching the junction and eventually maximizes at the junction, whose diameter is about 100 nm for the particular probe used. Since the temperature peaks sharply at the junction (where the thermoelectric signal is measured), this technique is very close to a point-heating and point-sensing scheme, which is ideal for local measurement.

In order to measure the local thermal conductivity with eq 14 in the active mode, we need to determine C/a and a dimensionless constant C/G_{ts}. To do so, we rewrite eq 14 as

$$T_c = \left[\left(\frac{C}{4a}\right)\frac{1}{k} + \frac{C}{G_{ts}}\right](T_{nc} - T_c) + T_\infty \quad (16)$$

and determine these two constants experimentally from the proportionality of T_c with respect to $T_{nc} - T_c$, as shown in Figure 6a. Silicon and Pyrex glass were used as the samples, for their thermal properties are well-known. Though, in general, G_{ts} depends on the sample properties and can vary from one sample to another, we assume that, due to its native oxide, the surface properties of silicon are very similar to those of Pyrex glass, whose major composition is amorphous silicon oxide. For the particular probe and the samples, C/a and C/G_{ts} were 79.76 W/m·K and 13.5 K/K, respectively.

To check the resolution in the depth direction, we measured the effective thermal conductivity of 25 to 1800 nm thick silicon oxide films grown on a silicon substrate. Due to the large thermal conductivity of the silicon substrate (~140 W/m·K), the measured values for 25 nm thick and 50 nm thick oxide films are larger than the bulk value of silicon oxide. Nevertheless, the measured value for 100 nm thick oxide film approaches the bulk value, as shown in Figure 6b. By comparing the measured value with the theoretical curves,[26] the thermal contact radius for the particular probe is estimated to be around 25 nm.

To demonstrate the thermal conductivity profiling in the lateral direction, we need a sample whose lateral thermal conductivity distribution is well-known and suitable for testing the limit regarding the spatial resolution. A few samples, in which a thin silicon oxide layer is sandwiched between single-crystal silicon layers, as depicted in Figure 6, were fabricated and used. For the sample with a 200 nm wide oxide layer, the measured T_c and T_{nc} and the k^{-1} derived from them through eq 14 are shown in Figure 6c; those for the 100 nm wide oxide layer are displayed in Figure 6d.

For the 200 nm wide sample, the measured effective thermal conductivity reaches the bulk value of silicon oxide at the middle of the oxide region. For the 100 nm wide sample, however, even though the tip–sample thermal contact is made within the oxide region (the thermal contact radius for the particular probe is around 25 nm), the measured thermal conductivity is rather higher than the bulk value. This is because the thermal conductivity is estimated from the spreading thermal resistance, which is influenced by the high thermal conductivity of the surrounding single-crystal silicon layers.

Finally, we need to discuss and analyze the measurement accuracy and temporal and spatial resolution of the method developed in this study. One of the important questions concerning the quantitative measurement of the temperature with SThM is whether the temperature of the sample will be disturbed by Q_{ts}. Whenever the temperature is measured by SThM, there always exists Q_{ts}, unless it is nullified artificially. As long as Q_{ts} exists, the temperature of the sample will suffer some disturbance, however small.

In order to evaluate Q_{ts}, G_{ts} should first be estimated. In general, G_{ts} depends on the radius of the tip and the surface properties of the sample. A rigorous estimation of G_{ts} was done for an SThM probe whose tip radius is quite close to the one used in this study and a sample whose constituent materials are the same as those used in this study.[15] According to this previous study, G_{ts} is ~20 nw/K.

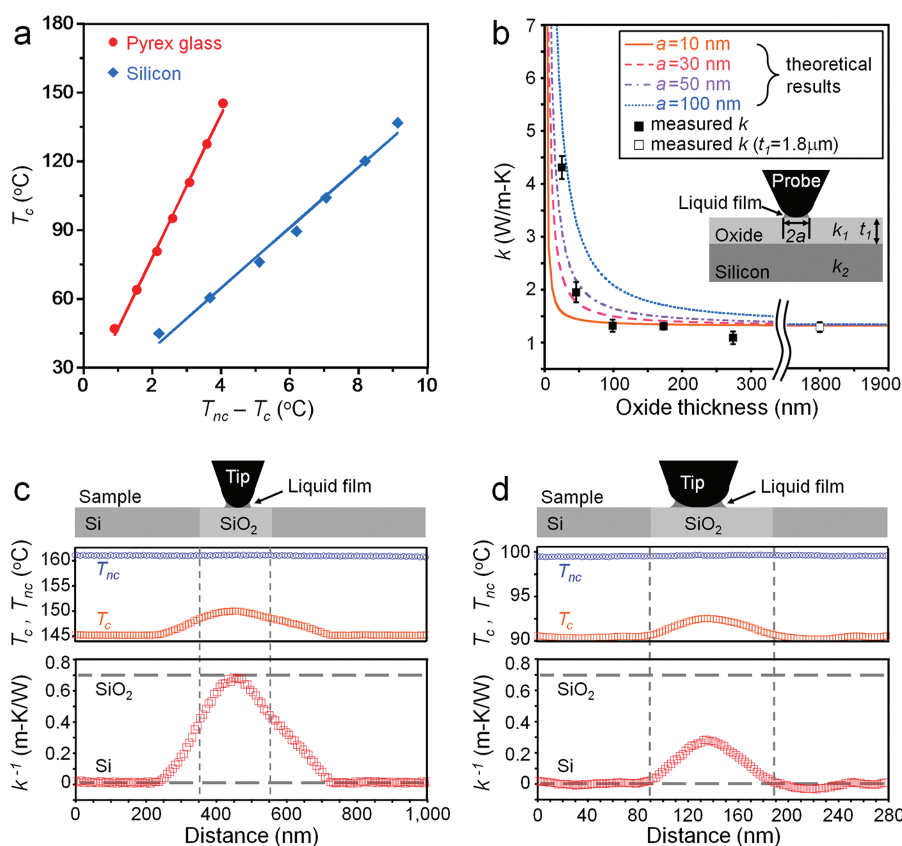

Figure 6. Demonstration of quantitative thermal conductivity profiling. (a) Calibration of the SThM probe for quantitative thermal profiling. From the proportionality of T_c with respect to $T_{nc} - T_c$ for silicon and Pyrex glass, whose thermal conductivities are well-known, C/a and C/G_{ts} are determined. (b) Effective thermal conductivity of the silicon oxide film grown on the silicon substrate as a function of the film thickness. (c) Structure of the sample for demonstrating the lateral resolution (top). The measured T_c and T_{nc} (center). The effective k^{-1} derived from the measured T_c and T_{nc} through eq 7 for the 200 nm wide sample (bottom). (d) Figure and graphs for the 100 nm wide sample corresponding to those in panel c. The error bars are calculated from the standard deviation of the measured thermal conductivity.

Once Q_{ts} is evaluated with eq 11, the temperature rise or drop due to Q_{ts} can be estimated with eq 13. Hence, the perturbation of the temperature, ΔT_{err}, due to Q_{ts} can be written as

$$\Delta T_{err} \approx R_{th} Q_{ts} = \frac{G_{ts}(T_c - T_s)}{4ak} \quad (17)$$

Now, if the maximum values of T_c and T_s in the silicon oxide region of Figure 4b, a as estimated from Figure 6b, and k of silicon oxide are substituted into eq 17, ΔT_{err} is estimated to be ∼−0.85 K. Since the room temperature during the measurement is 23.5 °C, the temperature measurement error is ∼−8%.

However, ΔT_{err} would be less than this because $T_c - T_s$ used in this estimation is not the actual temperature difference across the thermal contact but the one between the thermocouple junction and the sample surface, which should be much larger than the actual value. This estimation shows that care should be taken if the local thermal spreading resistance of the sample surface is large.

The temporal resolution of the method is determined by the time constant of the SThM probe, which was estimated to be ∼1 ms by Rho *et al.*[25] The time constant of the probe limits the scan rate, which should be controlled so that the dwelling time of the probe at each data point is at least several milliseconds.

The best spatial resolution of the method is bounded by the diameter of the tip−sample thermal contact area, which is estimated to be ∼50 nm from Figure 6b. However, the actual spatial resolution is also limited by the temperature gradient of the sample and the measurement noise of the SThM probe. The relation between the spatial resolution, the temperature gradient, and the measurement noise can be shown to be

$$\Delta x = \frac{\varphi \cdot \Delta T_{NE}}{(dT/dx)} = \frac{\varphi}{(dT/dx)} \frac{\Delta V_N}{S} = \frac{\varphi}{(dT/dx)} \frac{\sqrt{4k_B T R \Delta f}}{S} \quad (18)$$

where Δx is the spatial resolution, ΔT_{NE} is the noise equivalent temperature measured by the thermocouple probe, ΔV_N, S, R, and Δf are the noise equivalent voltage, thermopower, electrical resistance, and bandwidth of the probe, respectively, and k_B is the Boltzmann constant. In case of the SThM probe used in this study, φ is ∼10, S is 18.58 V/K, R is 500 Ω, Δf is 1 kHz,

and the resulting ΔV_N is ~0.1 V. Since dT/dx in Figure 4b is ~10^6 K/m, the resulting Δx is also ~50 nm.

CONCLUSION

In this study, we identified and amplified on the nonlocal nature of measurement by conventional SThM, which prevents quantitative temperature and thermal conductivity profiling. Then, we established a rigorous but simple and effective theory for quantitative SThM and verified it with high-performance SThM probes. Though the spatial resolution of the current experimental results was limited by the tip−sample contact diameter, with further reduction of the tip radius and improvement in the sensitivity of SThM probe, the performance of the quantitative SThM can be improved much further.

The establishment of high-performance quantitative SThM will enable new breakthroughs in many areas of nanothermal science and engineering: the thermal characterization of nanomaterials such as graphene,[27−30] carbon nanotubes, nanowires, and superlattices, which still remains hopelessly tricky and difficult; and the experimental analysis of thermal phenomena in nanoelectronic devices such as silicon-on-insulator nanotransistors,[31] light-emitting diodes, and carbon nanotube devices, which has depended mostly on theoretical analysis without proper experimental verification.

METHODS

Finite Element Modeling. We used the PDE Toolbox of MATLAB to model the temperature distribution around the 300 nm wide gold heater line. The sample in the computational domain was a 300 nm wide and 25 nm thick gold line patterned on a 1.8 μm thick silicon oxide layer grown on a silicon substrate (1 cm wide × 500 μm thick). The thermal conductivities of silicon oxide, silicon, and gold were set to 1.4, 150, and 317 W/m·K, respectively. Heat convection to the air from the top of the sample was neglected. The temperature at the boundaries except the top surface was set to zero. After the temperature profile was obtained, the profile was shifted until the temperature of the heater itself matched with the temperature measured by the TCR of the heater line, T_{TCR}. The temperature shift was 24.5 °C, which was quite close to the room temperature during the measurement (23.5 °C).

SThM Measurements. Scanning thermal microscopy was performed on an atomic force microscope (MultiMode operated with a Nanoscope IIIa controller, Digital Instruments/Veeco). For the nonthermal contact mode, "Lift mode" among the "Interleave modes" was used in the control program offered from Veeco. In Lift mode, AFM first gets the topographic data through scanning in contact, and then the probe scans the sample at a constant height above the sample using the topographic data obtained from the first scan. In order to make sure the probe scans at the right height above the sample, a force calibration test is performed before and after the scans.

Acknowledgment. This work was supported by a Korea Research Foundation grant (KRF-2007-313-D00089) and a National Research Foundation of Korea grant (2010-0014522) funded by the Korea government. The authors thank the Interuniversity Semiconductor Research Center (ISRC) at Seoul National University.

Supporting Information Available: Details of batch fabrication of the full dioxide thermocouple SThM probe and method of finite element modeling. This material is available free of charge *via* the Internet at http://pubs.acs.org.

REFERENCES AND NOTES

1. Majumdar, A. Scanning Thermal Microscopy. *Annu. Rev. Mater. Sci.* **1999**, *29*, 505–585.
2. Pollock, H. M.; Hammiche, A. Micro-Thermal Analysis: Techniques and Applications. *J. Phys. D: Appl. Phys.* **2001** *34*, R23–R53.
3. Lai, J.; Chandrachood, M.; Majumdar, A.; Carrejo, J. P. Thermal Detection of Device Failure by Atomic-Force Microscopy. *IEEE Electron Device Lett.* **1995**, *16*, 312–315.
4. Fiege, G. B. M.; Feige, V.; Phang, J. C. H.; Maywald, M.; Gorlich, S.; Balk, L. J. Failure Analysis of Integrated Devices by Scanning Thermal Microscopy (SThM). *Microelectron. Reliab.* **1998**, *38*, 957–961.
5. Fiege, G. B. M.; Niedernostheide, F. J.; Schulze, H. J.; Barthelmess, R.; Balk, L. J. Thermal Characterization of Power Devices by Scanning Thermal Microscopy Techniques. *Microelectron. Reliab.* **1999**, *39*, 1149–1152.
6. Kwon, O.; Majumdar, A. Cross-Sectional Thermal Imaging of a Metal-Oxide-Semiconductor Field-Effect Ttransistor. *Microscale Thermophys. Eng.* **2003**, *7*, 349–354.
7. Boroumand, F. A.; Voigt, M.; Lidzey, D. G.; Hammiche, A.; Hill, G. Imaging Joule Heating in a Conjugated-Polymer Light-Emitting Diode Using a Scanning Thermal Microscope. *Appl. Phys. Lett.* **2004**, *84*, 4890–4892.
8. Luo, K.; Herrick, R. W.; Majumdar, A.; Petroff, P. Scanning Thermal Microscopy of a Vertical-Cavity Surface-Emitting Laser. *Appl. Phys. Lett.* **1997**, *71*, 1604–1606.
9. Choi, S. H.; Lee, T. I.; Baik, H. K.; Roh, H. H.; Kwon, O.; Suh, D. H. The Effect of Electrode Heat Sink in Organic-Electronic Devices. *Appl. Phys. Lett.* **2008**, *93*, 183301.
10. Hammiche, A.; Bozec, L.; Conroy, M.; Pollock, H. M.; Mills, G.; Weaver, J. M. R.; Price, D. M.; Reading, M.; Hourston, D. J.; Song, M. Highly Localized Thermal, Mechanical, and Spectroscopic Characterization of Polymers Using Miniaturized Thermal Probes. *J. Vac. Sci. Technol., B* **2000**, *18*, 1322–1332.
11. Hammiche, A.; Hourston, D. J.; Pollock, H. M.; Reading, M.; Song, M. Scanning Thermal Microscopy: Subsurface Imaging, Thermal Mapping of Polymer Blends, and Localized Calorimetry. *J. Vac. Sci. Technol., B* **1996**, *14*, 1486–1491.
12. Nelson, B. A.; King, W. P. Measuring Material Softening with Nanoscale Spatial Resolution Using Heated Silicon Probes. *Rev. Sci. Instrum.* **2007**, *78*, 023702.
13. Shi, L.; Plyasunov, S.; Bachtold, A.; McEuen, P. L.; Majumdar, A. Scanning Thermal Microscopy of Carbon Nanotubes Using Batch-Fabricated Probes. *Appl. Phys. Lett.* **2000**, *77*, 4295–4297.
14. Shi, L.; Zhou, J. H.; Kim, P.; Bachtold, A.; Majumdar, A.; McEuen, P. L. Thermal Probing of Energy Dissipation in Current-Carrying Carbon Nanotubes. *J. Appl. Phys.* **2009**, *105*, 104306.
15. Shi, L.; Majumdar, A. Thermal Transport Mechanisms at Nanoscale Point Contacts. *J. Heat Transfer* **2002**, *124*, 329–337.
16. Luo, K.; Shi, Z.; Varesi, J.; Majumdar, A. Sensor Nanofabrication, Performance, and Conduction Mechanisms in Scanning Thermal Microscopy. *J. Vac. Sci. Technol., B* **1997**, *15*, 349–360.
17. Ruiz, F.; Sun, W. D.; Pollak, F. H.; Venkatraman, C. Determination of the Thermal Conductivity of Diamond-like Nanocomposite Films Using a Scanning Thermal Microscope. *Appl. Phys. Lett.* **1998**, *73*, 1802–1804.

18. Kwon, O.; Shi, L.; Majumdar, A. Scanning Thermal Wave Microscopy (STWM). *J. Heat Transfer* **2003**, *125*, 156–163.
19. Grosse, K. L.; Bae, M. H.; Lian, F. F.; Pop, E.; King, W. P. Nanoscale Joule Heating, Peltier Cooling and Current Crowding at Graphene-Metal Contacts. *Nat. Nanotechnol.* **2011**, *6*, 287–290.
20. Majumdar, A.; Varesi, J. Nanoscale Temperature Distributions Measured by Scanning Joule Expansion Microscopy. *J. Heat Transfer* **1998**, *120*, 297–305.
21. Reddy, P.; Sadat, S.; Tan, A.; Chua, Y. J. Nanoscale Thermometry Using Point Contact Thermocouples. *Nano Lett.* **2010**, *10*, 2613–2617.
22. Kim, K.; Chung, J.; Won, J.; Kwon, O.; Lee, J. S.; Park, S. H.; Choi, Y. K. Quantitative Scanning Thermal Microscopy Using Double Scan Technique. *Appl. Phys. Lett.* **2008**, 93.
23. Carslaw, H. S.; Jaeger, J. C. *Conduction of Heat in Solids*, 2nd ed.; Clarendon Press: Oxford, 1986; p viii, 510 pp.
24. Roh, H. H.; Lee, J. S.; Kim, D. L.; Park, J.; Kim, K.; Kwon, O.; Park, S. H.; Choi, Y. K.; Majumdar, A. Novel Nanoscale Thermal Property Imaging Technique: The 2 Omega Method. I. Principle and the 2 Omega Signal Measurement. *J. Vac. Sci. Technol., B* **2006**, *24*, 2398–2404.
25. Roh, H. H.; Lee, J. S.; Kim, D. L.; Park, J.; Kim, K.; Kwon, O.; Park, S. H.; Choi, Y. K.; Majumdar, A. Novel Nanoscale Thermal Property Imaging Technique: The 2 Omega Method. II. Demonstration and Comparison. *J. Vac. Sci. Technol., B* **2006**, *24*, 2405–2411.
26. Dryden, J. R. The Effect of a Surface Coating on the Constriction Resistance of a Spot on an Infinite Half-Plate. *J. Heat Transfer* **1983**, *105*, 408–410.
27. Balandin, A. A.; Ghosh, S.; Bao, W. Z.; Calizo, I.; Teweldebrhan, D.; Miao, F.; Lau, C. N. Superior Thermal Conductivity of Single-Layer Graphene. *Nano Lett.* **2008**, *8*, 902–907.
28. Ghosh, S.; Bao, W. Z.; Nika, D. L.; Subrina, S.; Pokatilov, E. P.; Lau, C. N.; Balandin, A. A. Dimensional Crossover of Thermal Transport in Few-Layer Graphene. *Nat. Mater.* **2010**, *9*, 555–558.
29. Seol, J. H.; Jo, I.; Moore, A. L.; Lindsay, L.; Aitken, Z. H.; Pettes, M. T.; Li, X. S.; Yao, Z.; Huang, R.; Broido, D.; Mingo, N.; Ruoff, R. S.; Shi, L. Two-Dimensional Phonon Transport in Supported Graphene. *Science* **2010**, *328*, 213–216.
30. Faugeras, C.; Faugeras, B.; Orlita, M.; Potemski, M.; Nair, R. R.; Geim, A. K. Thermal Conductivity of Graphene in Corbino Membrane Geometry. *ACS Nano* **2010**, *4*, 1889–1892.
31. Narumanchi, S. V. J.; Murthy, J. Y.; Amon, C. H. Comparison of Different Phonon Transport Models for Predicting Heat Conduction in Silicon-on-Insulator Transistors. *J. Heat Transfer* **2005**, *127*, 713–723.